

Comparison of light intensity on the brain surface due to laser exposure during optical topography and solar irradiation

Masashi Kiguchi

Hitachi, Ltd.
Advanced Research Laboratory
Hatoyama, Saitama 350-0395, Japan
and
Tokyo Institute of Technology
Graduate School of Science and Engineering
2-12-1 Ookayama, Meguro-ku
Tokyo 152-8550, Japan
E-mail: masashi.kiguchi.py@hitachi.com

Noriyoshi Ichikawa

Hitachi Medical Corporation
Medical System Operations Group
2-1 Shintoyofuta, Kashiwa-shi
Chiba 277-8678, Japan

Hirokazu Atsumori

Hitachi, Ltd.
Advanced Research Laboratory
Hatoyama, Saitama 350-0395, Japan
and
Tokyo Institute of Technology
Graduate School of Science and Engineering
2-12-1 Ookayama, Meguro-ku
Tokyo 152-8550, Japan

Fumio Kawaguchi

Hitachi Medical Corporation
Medical System Operations Group
2-1 Shintoyofuta, Kashiwa-shi
Chiba 277-8678, Japan

Hiroki Sato

Atsushi Maki

Hideaki Koizumi

Hitachi, Ltd.
Advanced Research Laboratory
Hatoyama, Saitama 350-0395, Japan

1 Introduction

Near-infrared spectroscopy (NIRS) has been widely used in functional brain studies to observe cerebral oxygenation and hemodynamics changes.¹⁻⁵ The optical topography (OT) systems (based on NIRS using multiple optical probes in a reflection-type arrangement) have succeeded in imaging the brain activity.^{6,7} The OT system enables noninvasive measurement of the human brain function under a variety of conditions with little subject restriction, so it has been applied to

Abstract. Optical topography (OT), which is based on the near-infrared spectroscopy, is a powerful tool for observing brain activity noninvasively. To estimate the effect of laser exposure on the brain, photon-distribution profiles in bald heads of adults and neonates during the OT were calculated using the photon-diffusion equation. These calculations showed that although the absolute values of the intensity depend on details of the head model, the relative values of OT exposure to sunlight exposure were less sensitive to the model details. As an example, the light intensities on the brain surface during OT obtained by using a commercially available system were about 2% for adults and 3% for neonates of those values obtained under midday sunlight on a sunny day in midsummer. These values were obtained under the reasonable assumptions with a large safety factor.
© 2007 Society of Photo-Optical Instrumentation Engineers. [DOI: 10.1117/1.2804152]

Keywords: NIRS; laser safety; optical topography; photon-diffusion equation.

Paper 07025SSR received Jan. 18, 2007; revised manuscript received Apr. 24, 2007; accepted for publication Apr. 26, 2007; published online Nov. 13, 2007.

various fields such as psychology, cognitive science, brain science, and clinical medicine.⁸⁻¹² It has been especially used in infant research as a useful tool because of the advantages mentioned above.^{13,14}

Research involving human participants is ethically required to identify the safety and/or risk of the examinations for subjects. In the measurement of brain function using NIRS, a laser beam is irradiated into the scalp and a part of the diffused light reaches the cortex. Evaluating the effects of laser exposure on the human body is therefore important. Most commercially available NIRS instruments are classified according to the IEC (International Electrotechnical Commis-

Address all correspondence to Masashi Kiguchi, Advanced Research Laboratory, Hitachi, Ltd., 2520 Akanuma - Hatoyama, Saitama 350-0395, Japan; Tel: +81-492-96-6111; Fax: +81-492-96-6006; E-mail: masashi.kiguchi.py@hitachi.com

Table 1 Five-layer head models for adult and neonate (after Ref. 24).

		Scalp	Skull	CSF	Gray	White
Adult	Thickness (mm)	5.0	7.0	2.0	5.0	
	$\mu'_s(\text{mm}^{-1})$	1.9	1.6	0.01	2.2	9.1
	$\mu_a(\text{mm}^{-1})$	0.018	0.016	0.002	0.036	0.014
Neonate	Thickness (mm)	2.0	2.0	0.5	3.0	
	$\mu'_s(\text{mm}^{-1})$	1.9	1.6	0.01	0.5	1.0
	$\mu_a(\text{mm}^{-1})$	0.018	0.016	0.002	0.048	0.037

μ'_s : reduced scattering coefficient
 μ_a : absorption coefficient

sion) standard (IEC 60825-14),¹⁵ which expresses the safety of laser products against skin and eye hazards. As the IEC standard defines the maximum permissible exposure (MPE) values for skin and eyes according to biological considerations, it is possible to evaluate the safety regarding the scalp and eyes associated with using NIRS instruments. An assessment of heating effects in the skin during NIRS studies has been reported.¹⁶ However, no standard covers any brain hazards caused by laser exposure. So no MPE for the brain has been determined. The aim of this paper is thus to provide the scientific data to evaluate the safety of the brain during OT.

In the near-infrared region, most laser damage is due to heating of the absorbing tissues (IEC 60825-1).¹⁷ A rise in brain temperature due to the laser exposure may be calculated by using a light-propagation simulation and a heat-diffusion model. However, calculating the absolute values of light intensity and temperature is extremely difficult because the values of the tissue parameters to put into the simulation are difficult to obtain accurately. We therefore calculated the light intensity on the brain surface during both OT and the equivalent normal exposure the sun and compared the two intensities to estimate the effect of the OT. This approach does not directly estimate the temperature rise, but it has the following advantages. First, it does not need any thermal parameters for components in the head, for example, heat capacitances and heat resistances for the scalp, skull, brain, and such, which are difficult to obtain. Second, reducing the number of parameters increases the reliability of results. Third, relative results are less sensitive to the errors in parameters and variation in the model than absolute results. Fourth, comparing exposure under OT with that under sunlight, which we are exposed to daily, helps to intuitively evaluate the safety of observing the brain with OT.

The photon-diffusion equation has been used for calculating photon-propagation profiles in scattering media such as biological tissues.¹⁸⁻²² Light propagation in the head was calculated by the photon-diffusion equation with three-dimensional head models for adults and neonates. Because the photon-diffusion equation is based on the strong-scattering approximation, it may be unacceptable to use it for the head model including a clear cerebrospinal fluid (CSF) layer.²³ We therefore performed the calculations using two models, one including a CSF layer and one without a CSF layer.

2 Calculations

The structures and optical properties of the adult and neonatal head models are given in Table 1.²¹ The five-layer head model consisted of scalp, skull, CSF, gray matter, and white matter. In the four-layer head model, the skull replaced the CSF layer. The hair was not included in either model. This assumption is reasonable for bald adults and also acceptable for most neonates, who are almost bald or have thin hair. Because the head has a spherical shape, we used the spherical-polar coordinates system for the calculations. The adult head was modeled as a sphere with a diameter of 180 mm and the neonatal head as a sphere with a diameter of 100 mm; both consisted of the layers as shown in Table 1. The wavelength dependence of the optical properties was not considered because there is little information on this in the literature.

The photon-diffusion equations are written as

$$\frac{1}{c} \frac{\partial \Phi(\mathbf{r}, t)}{\partial t} - \text{div}\{D(\mathbf{r}) \text{grad } \Phi(\mathbf{r}, t)\} + \mu_a(\mathbf{r})\Phi(\mathbf{r}, t) = q_0(\mathbf{r}, t),$$

$$D(\mathbf{r}) = 1/\{3[\mu'_s(\mathbf{r}) + \mu_a(\mathbf{r})]\} \quad (1)$$

where $\Phi(r)$, μ'_s and μ_a are the photon-fluence rate, the reduced scattering coefficient, and absorption coefficient, respectively. $D(r)$ is defined as the diffusion coefficient.

Both sides are integrated as

$$\int \frac{1}{c} \frac{\partial \Phi}{\partial t} dv + \oint \mathbf{n}(D \text{grad } \Phi) ds + \int \mu_a \Phi dv = \int q_0 dv, \quad (2)$$

where

$$\int \frac{1}{c} \frac{\partial \Phi}{\partial t} dv = \frac{1}{c} \frac{\Phi - \Phi^{old}}{\Delta t} \Delta v = \frac{1}{c} \frac{\Phi - \Phi^{old}}{\Delta t} r^2 \sin \theta dr d\theta d\varphi,$$

$$\int \mu_a \Phi dv = \mu_a \Phi r^2 \sin \theta dr d\theta d\varphi. \quad (3)$$

As no optical source exists in the head,

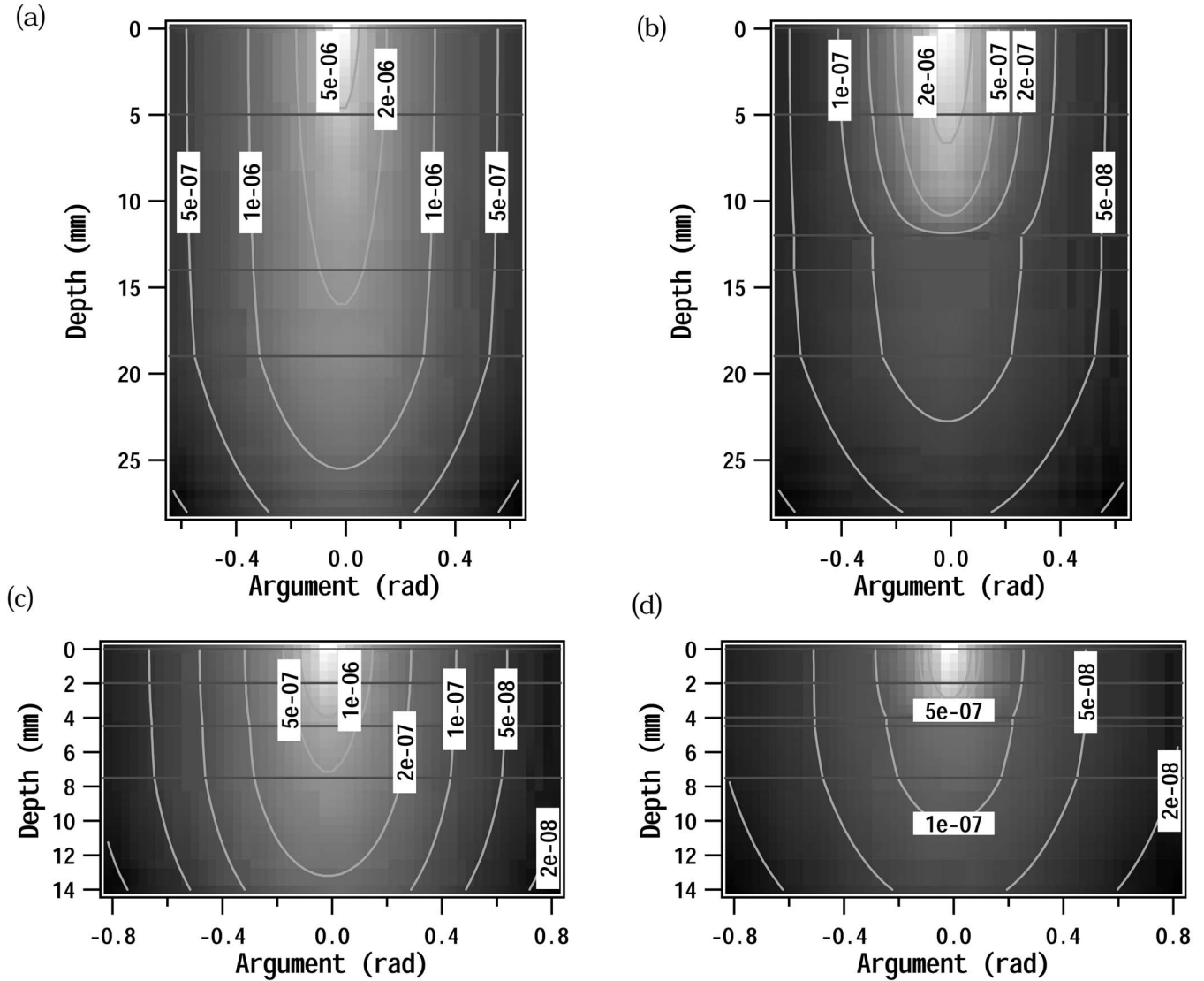


Fig. 1 Distributions of the photon-fluence rate (Φ) in the head calculated using (a) adult four-layer model, (b) adult five-layer model, (c) neonatal four-layer model, and (d) neonatal five-layer model. A single optical source was placed on the scalp.

$$\int q_0 dv = 0. \quad (4)$$

For the truncated boundary ξ , we used a self-consistent boundary condition

$$\Phi(\xi + \Delta)/\Phi(\xi) = \Phi(\xi + 2\Delta)/\Phi(\xi + 2\Delta) = \text{Const}. \quad (5)$$

The value of *Const* was obtained by iterative calculations for each boundary. This boundary condition provides less distorted distributions of Φ than the Dirichlet condition, $\Phi(\xi) = 0$.²⁵

For the boundary ξ_s between the scalp and air, the modified Robin-type boundary condition²¹ was used as

$$\Phi(\xi_s) + 2D(\xi_s)A\hat{\mathbf{n}} \cdot \nabla\Phi(\xi_s) = 0. \quad (6)$$

Here, $\hat{\mathbf{n}}$ is the unit vector normal to the boundary and $A = 2.4$ for the boundary between air, whose refractive index is

1, and the biological tissue, whose refractive index is 1.4.¹⁸ The source was placed at the boundary of the scalp ξ_s^l . The Robin boundary condition was then used at the source as follows:²¹

$$\Phi(\xi_s^l, t) + 2D(\xi_s^l)A\hat{\mathbf{n}} \cdot \nabla\Phi(\xi_s^l, t) = -4\Gamma_S w(\xi_s^l, t), \quad (7)$$

with the distribution function of the source, $w(\xi_s^l, t)$, and the flow rate of incident light Γ_S . We consider here a continuous-wave source uniformly distributed across the source area. Therefore, Φ and w are independent of time and $w = 1$. The source area was $1 \times 1 \text{ mm}^2$.

The equations were solved by the finite-difference method using $0.5 \text{ mm} \times 0.1 \text{ rad} \times 0.1 \text{ rad}$ meshes.

3 Results and Discussion

Figure 1 shows the distributions in the four-layer and five-layer head models for the adults and neonates. The distribu-

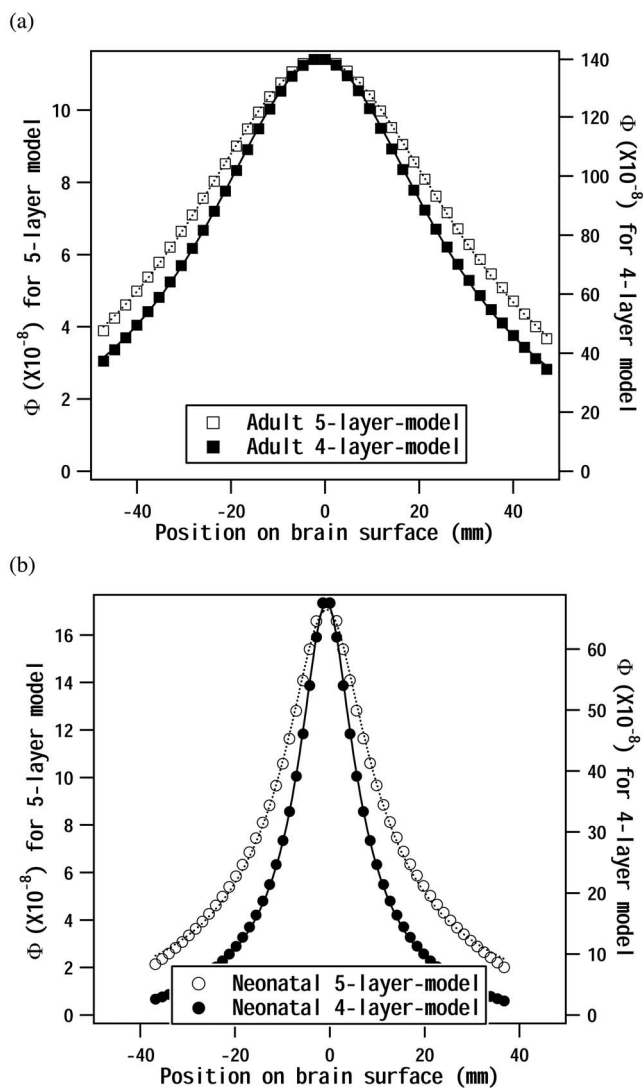


Fig. 2 Profiles of the photon-fluence rate (Φ) in the gray matter irradiated by the single source for (a) an adult and (b) a neonate. The depths of the irradiated area from the scalp surface were (a) 15 mm and (b) 5 mm, respectively. The horizontal axis shows the position along the brain curvature from the point just under the source. Markers represent the results of calculation, and curves were obtained by the least-squares fitting with a theoretical function.

tion patterns were affected by the existence of the CSF layers. The light-distribution profiles on the brain surface, that is, the gray-matter layer, for the respective models are shown in Fig. 2. The depths of the gray matter from the scalp surface were 15 mm for the adults and 5 mm for the neonates. The horizontal axis represents the distance along the surface of the gray matter from the source. The origin was right under the source. The circles represent the calculated results. Comparing the four- and five-layer models shows that the CSF layer made the light spread over a wider area in the gray matter. The lines in the figure were obtained by least-squares fitting with

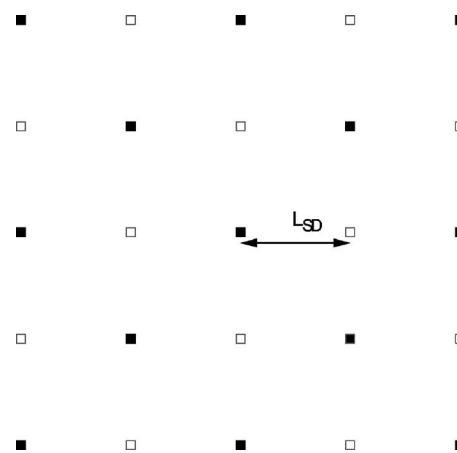


Fig. 3 Probe geometry used in the calculation for the OT. Opaque and open squares represent the sources and the detectors, respectively. L_{SD} is the SD distance.

$$f(x, y, x_0, y_0) = \frac{A \exp\sqrt{(x-x_0)^2 + (y-y_0)^2 + z_0^2}}{\sqrt{(x-x_0)^2 + (y-y_0)^2 + z_0^2}}, \quad (8)$$

where $f(x, y, x_0, y_0)$ is a distribution function of light in the gray matter, when a single source (area: $1 \times 1 \text{ mm}^2$) is placed at a position $(x, y) = (x_0, y_0)$ on the scalp. This equation can easily be expanded to cover multiple sources. The distribution of total light in the gray matter was obtained as $\sum_i f(x, y, x_i, y_i)$ with all source positions, i s. The simple addition of distribution functions is reasonable, because the light is strongly scattered and interference light is negligible. Usually in OT, multiple probes of sources and detectors are arranged in a lattice form for obtaining a topographic image of brain activity. The calculations were performed using the probe geometry shown in Fig. 3 with the distances between the source and detector (SD distances, L_{SD}) set at 20, 30, and 40 mm, respectively. The opaque squares in Fig. 3 represent the sources and the open squares represent the detectors, which were not used in the calculations. In the case of solar irradiation, the sources were uniformly distributed on the scalp.

Both results are compared in Fig. 4, which shows $\Phi[\text{probe}]$ and $\Phi[\text{uniform}]$ corresponding to the distributions of light in the gray matter during the OT and under sunlight, respectively. Because the gray matter was shallow in the neonatal head models, the photons did not become fully diffuse and the $\Phi[\text{probe}]$ values had a peak directly under the probe position. When the SD distance was shorter, the peak was steeper and the peak value was larger, because the neighboring sources were closer. Although $\Phi[\text{uniform}]$ should ideally be flat, it varies slightly due to the limited calculation area. However, this variation was not a problem, because we paid attention to the peak value of Φ at the origin. The intensity in the case of the multiple-probe irradiation was much smaller than the intensity in the case of the uniform irradiation. This is because the incident power per unit square was the same in both cases and the area of scalp irradiated in the uniform case was overwhelmingly larger than the total area of the incident probes.

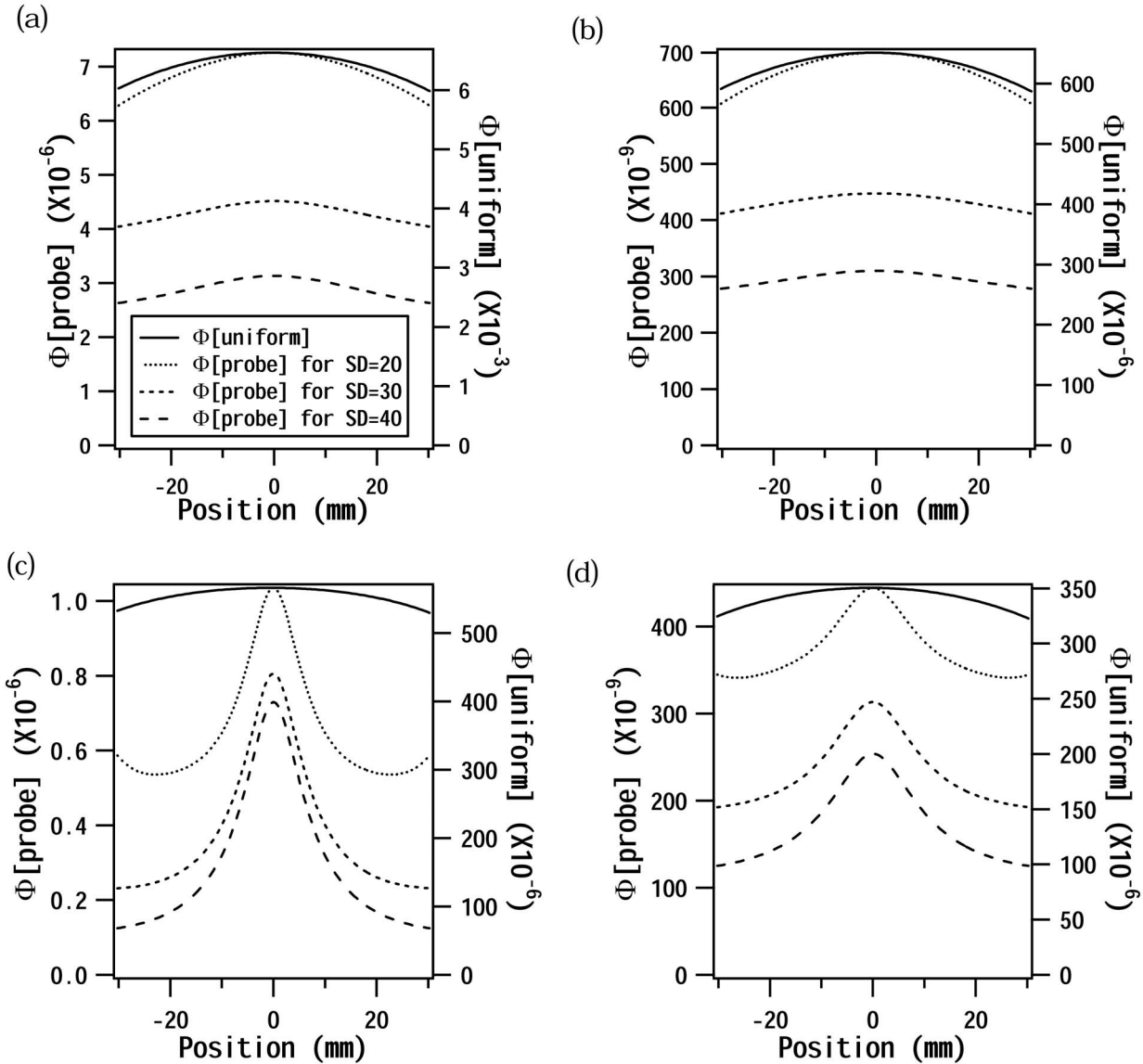


Fig. 4 Profiles of the photon-fluence rate (Φ) in the gray matter calculated using (a) adult four-layer model, (b) adult five-layer model, (c) neonatal four-layer model, and (d) neonatal five-layer model. $\Phi[probe]$ was obtained by using multiple sources as the OT, and $\Phi[uniform]$ was obtained with sources uniformly distributed on the scalp surface.

In the above, unit incidences were assumed for both the probe and the uniform cases; in the following, the actual power irradiated during OT and the actual solar power are introduced. The incident power for the probe irradiation ($I[OT]$) was determined to be 1 mW/mm^2 , for simplicity. For sunlight, the solar spectral irradiance (ASTM E891-87) was used.²⁶ The total intensity of the midday sunlight on a sunny day in midsummer is set at 1000 W/m^2 in the standard. Because the wavelength dependence of both the scattering and absorption coefficients of tissue in the wavelength range between 700 and 850 nm, which are typical wavelengths of light sources in an OT system, is small,²⁷ in the case of sunlight we assumed that only the intensity integrated over the range of wavelengths from 700 to 850 nm ($I[sun]$) was irradiated. From the solar spectral irradiance,

$$I[sun] = 165 \text{ W/m}^2. \tag{9}$$

The ratio of light intensity in the gray matter during OT ($\Phi[OT]$) to that under sunlight ($\Phi[sun]$) is given as

$$\Phi[OT]/\Phi[sun] = \Phi[probe]/\Phi[uniform] \times I[OT]/I[sun]. \tag{10}$$

Figure 5 shows the results of Eq. (10) for each head model and each SD distance. Although the values of Φ in the gray matter in Fig. 4 differ from according to the model, the ratios in Fig. 5 were less sensitive to the model details. This relative comparison therefore reduced the error caused by the uncertainty of the models.

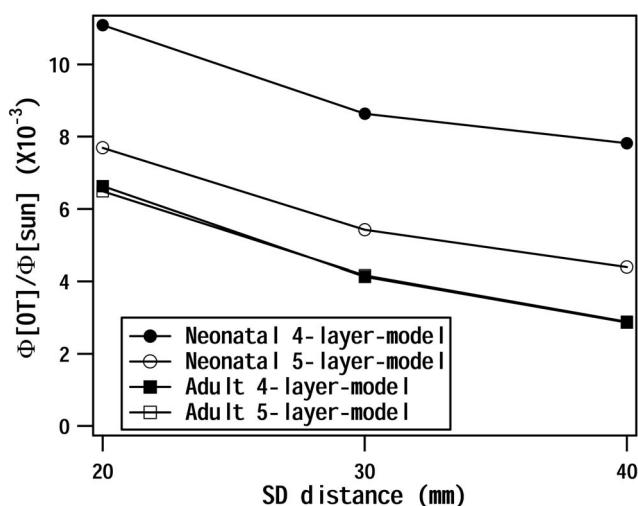


Fig. 5 Ratios of the photon-fluence rate (Φ) in the gray matter during OT compared to those during exposure to sunlight. The output power from each source probe was 1 mW. The solar spectral irradiance and the total intensity of the midday sunlight on a sunny day in midsummer were given by ASTM E-891.

The ratios were calculated using the peak values of $\Phi[OT]$ at the origin. The value that affects the temperature rise is the mean value of $\Phi[OT]$ over a wider area. When the mean values are used, the ratios in Fig. 5 become smaller. The incident intensity of the sunlight must be larger in actual fact, because solar energy has a wide distribution from ultraviolet to infrared, and the wavelength range of light penetration into the head is much wider than that used in the above calculation. In this case, the ratios also become smaller. All of these mean that the effect of OT relative to the effect of actual sunlight is less than that calculated above. It can therefore be concluded that the ratios shown in Fig. 5 were estimated with a large safety factor.

The models used above included no hair. Because hair might shade the sunlight more effectively than the light from the probes, the ratios in Fig. 5 might become larger when hair is taken into consideration. It was, however, difficult to incorporate the effect of hair into the model quantitatively, because the amount and color of hair vary greatly across individuals. The results obtained above are valid for bald or very thin-hair heads and, at least, frontal head positions. The construction of a model including hair is thus desirable for more general investigations.

We apply the above results to a commercially available system, the ETG-100 (Hitachi, Medical Corporation, Japan), as an example of an actual case. The probe output power of ETG-100 can be set to three levels, the highest of which from each source probe is 3 mW. When this setting is used, the ratios in Fig. 5 should be multiplied by 3. Considering the photon spread due to the CSF layer,²⁴ the five-layer model might be closer to the actual head than the four-layer model. However, the photon-diffusion equation might not be valid for the model including the clear CSF layer and reality must lie somewhere between the result for four-layer model and that for the five-layer model. Therefore, we took the four-layer model as the possible worst case. The light intensity in the

gray matter during a measurement using ETG-100 for the adult and the neonate were about 1.2 and 2.6% of that under sunlight, respectively, when the SD distances were set at 30 mm as usual. They were 2.0 and 3.3%, respectively, when the SD distances were set at 20 mm, which is the condition sometimes used for infants. Therefore, it is concluded that the ratios of the light intensity on the brain surface during OT using ETG-100 with the SD distances of 20 or 30 mm compared to those during exposure to sunlight were about 2% for the adult and 3% for the neonate, respectively. In the case of sunlight on a cloudy day in winter (the total solar intensity is 150 W/m^2), the above ratios become 13 and 22%, respectively.

4 Conclusions

To evaluate the effect of light exposure to the brain during OT, the light intensity on the brain surface during OT—calculated by using the photon-diffusion equation with adult and neonatal head models (with no hair)—were compared with that obtained under sunlight.

The intensities on the brain surface during OT (using an ETG-100 with a probe output of 3 mW and the lattice form of probe geometry with each SD distance of 20 or 30 mm) were about 2% for adults and 3% for neonates of those intensities under midday sunlight on a sunny day in midsummer, respectively. These values were obtained using the acceptable assumptions with a large enough safety factor. The effect of OT on the brain was thus estimated to be far less than the effect of the sunlight.

Because the MPE for the brain was not known, we cannot yet declare the safety level for OT. Also effects of sunlight for bald neonates should be quantitatively considered. The safety should be evaluated by a variety of medical and engineering inspections and considerations. However, the comparison of irradiation by OT with that of natural sunlight will help us to evaluate the safety of OT.

Acknowledgments

Parts of this research were financially supported by Core Research for Evolutional Science and Technology, Japan Science and Technology Agency and Brain Development and the Life Long Learning Network program of RIKEN.

References

1. F. F. Jobsis, "Noninvasive infrared monitoring of cerebral and myocardial sufficiency and circulatory parameters," *Science* **198**, 1264–1267 (1977).
2. B. Chance, Z. Zhuang, C. C. Unah, C. Alter, and L. Lipton, "Cognition-activated low-frequency modulation of light absorption in human brain," *Proc. Natl. Acad. Sci. U.S.A.* **90**, 3770–3774 (1993).
3. A. Villringer, J. Planck, C. Hock, L. Schleinkofer, and U. Dirnagl, "Near infrared spectroscopy (NIRS): A new tool to study hemodynamic changes during activation of brain function in human adults," *Neurosci. Lett.* **154**, 101–104 (1993).
4. Y. Hoshi and M. Tamura, "Detection of dynamic changes in cerebral oxygenation coupled to neuronal function during mental work in man," *Neurosci. Lett.* **150**, 5–8 (1993).
5. T. Kato, A. Kamei, S. Takashima, and T. Ozaki, "Human visual cortical function during photic stimulation monitoring by means of near-infrared spectroscopy," *J. Cereb. Blood Flow Metab.* **13**, 516–520 (1993).

6. A. Maki, Y. Yamashita, Y. Ito, E. Watanabe, H. Mayanagi, and H. Koizumi, "Spatial and temporal analysis of human motor activity using noninvasive NIR topography," *Med. Phys.* **22**, 1997–2005 (1995).
7. Y. Yamashita, A. Maki, and H. Koizumi, "Near-infrared topographic measurement system: Imaging of absorbers localized in a scattering medium," *Rev. Sci. Instrum.* **67**, 730–732 (1996).
8. E. Watanabe, A. Maki, F. Kawaguchi, K. Takashiro, Y. Yamashita, H. Koizumi, and Y. Mayanagi, "Non-invasive assessment of language dominance with near-infrared spectroscopic mapping," *Neurosci. Lett.* **256**, 49–52 (1998).
9. H. Sato, T. Takeuchi, and K. L. Sakai, "Temporal cortex activation during speech recognition: An optical topography study," *Cognition* **73**, B55–B66 (1999).
10. Y. Noguchi, T. Takeuchi, and K. L. Sakai, "Lateralized activation in the inferior frontal cortex during syntactic processing: Event-related optical topography study," *Hum. Brain Mapp* **17**, 89–99 (2002).
11. A. Obata, K. Morimoto, H. Sato, A. Maki, and H. Koizumi, "Acute effects of alcohol on hemodynamic changes during visual stimulation assessed using 24-channel near-infrared spectroscopy," *Psychiatry Res.: Neuroimag.* **123**(2), 145–152 (2003).
12. T. Suto, M. Fukuda, M. Itho, T. Uehara, and M. Mikuni, "Multichannel near-infrared spectroscopy in depression and schizophrenia: Cognitive brain activation study," *Biol. Psychiatry* **55**, 501–511 (2004).
13. G. Taga, Y. Konishi, A. Maki, T. Tachibana, M. Fujiwara, and H. Koizumi, "Spontaneous oscillation of oxy- and deoxy-hemoglobin changes with a phase difference throughout the occipital cortex of newborn infants observed using non-invasive optical topography," *Neurosci. Lett.* **282**, 101–104 (2000).
14. M. Pena, A. Maki, D. Kovacic, G. Dehaene-Lambertz, H. Koizumi, F. Bouquet, and J. Mehler, "Sounds and silence: An optical topography study of language recognition at birth," *Proc. Natl. Acad. Sci. U.S.A.* **100**(20), 11702–11705 (2003).
15. International Electrotechnical Commission "IEC 60825-14: 2004 Safety of laser products, Part 14: A user's guide," international standard (2004).
16. Y. Ito, R. P. Kennan, E. H. Watanabe, and H. Koizumi, "Assessment of heating effects in skin during continuous wave near infrared spectroscopy," *J. Biomed. Opt.* **5**, 387 (2000).
17. International Electrotechnical commission, IEC 60825-1," international standard (2001).
18. M. Keijzer, W. M. Star, and P. R. Storch, "Optical diffusion in layered media," *Appl. Opt.* **27**, 1820–1824 (1988).
19. S. R. Arridge, M. Schweiger, M. Hiraoka, and D. T. Delpy, "A finite element approach for modeling photon transport in tissue," *Med. Phys.* **20**, 299–309 (1993).
20. B. W. Pogue, M. S. Patterson, H. Jiang, and K. D. Paulsen, "Initial assessment of a simple system for frequency domain optical tomography," *Phys. Med. Biol.* **40**, 1709–1729 (1995).
21. M. Schweiger, S. R. Arridge, M. Hiraoka, and D. T. Delpy, "The finite element method for the propagation of light in scattering media: Boundary and source conditions," *Med. Phys.* **22**, 1779–1792 (1995).
22. M. Ono, Y. Kashio, M. Schweiger, H. Dehghani, S. R. Arridge, M. Firbank, and E. Okada, "Topographic distribution of photon measurement density function on the brain surface by hybrid radiosity-diffusion method," *Opt. Rev.* **7**, 426–431 (2000).
23. M. Firbank, S. R. Arridge, M. Schweiger, and D. T. Delpy, "An investigation of light transport through scattering bodies with non-scattering regions," *Phys. Med. Biol.* **41**, 767 (1996).
24. E. Okada, "The effect of superficial tissue of the head on spatial sensitivity profiles for near infrared spectroscopy and imaging," *Opt. Rev.* **7**, 375–382 (2000).
25. M. Kiguchi and H. Kawaguchi, "Self-consistent boundary condition for photon diffusion calculation," in *Proc. 26th Annu. Int. Conf. Eng. Med. Biol. Soc.*, IEEE, 1207–1209 (2004).
26. American Society for Testing and Materials (ASTM), "Designation: E891-87 (reapproved 1992). Standard tables for terrestrial direct normal solar spectral irradiance for air mass 1.5," standard (1992).
27. V. S. Hollis, T. Binzoni, and D. T. Delpy, "Non-invasive monitoring of brain tissue temperature by near infrared spectroscopy," *Proc. SPIE* **4250**, 470–481 (2001).